



**ICA 2013 Montreal**  
**Montreal, Canada**  
**2 - 7 June 2013**

## **Signal Processing in Acoustics**

### **Session 4pSP: Sampling Methods for Bayesian Analysis and Inversions in Acoustic Applications**

#### **4pSP9. A Bayesian based equivalent sound source model for a military jet aircraft**

**David M. Hart\*, Tracianne B. Neilsen, Kent L. Gee and Michael M. James**

**\*Corresponding author's address: Brigham Young University, Provo, UT 84606, [dmh1993@studentbody.byu.edu](mailto:dmh1993@studentbody.byu.edu)**

The two-source model for jet noise holds that turbulent mixing noise in jets is generated by uncorrelated, fine-scale (FSS) and partially correlated, large-scale (LSS) turbulent structures [Tam et al., *J. Fluid Mech.* 615, 253-292, (2008)]. The noise from an F-22A Raptor is modeled with an equivalent source consisting of two line arrays of monopole sources. These arrays, one correlated and one uncorrelated, with Rayleigh distributed amplitudes, account for both FSS and LSS sound propagation [J. Morgan, *J. Acoust. Soc. Am.* 129, 2442 (2011)]. The equivalent source parameters are selected based on Bayesian methods implemented with simulated annealing and fast Gibbs sampler algorithms. This method yields the best fit parameters, and the sensitivity of the solution is indicated by the generated posterior probability distributions. Analysis of the resulting equivalent sources shows that the directional, correlated line array has greater effect on the near field sound, and the sensitivity of the array's parameters increases as the frequency increases. This equivalent source model can generate results up to 2500 Hz and accurately predict both near field and far field measurements. The analysis suggests that the shape of the source distribution changes as the frequency increases. [Work sponsored by the Office of Naval Research.]

Published by the Acoustical Society of America through the American Institute of Physics

## INTRODUCTION

A better understanding of jet noise source characteristics from military jet aircraft is needed to more accurately model near and far-field propagation. Although researchers have investigated and determined features of jet turbulence in laboratory experiments,<sup>1,2</sup> properties of heated, supersonic jets from military aircraft cannot be directly measured. Computational models, both analytical<sup>3,4</sup> and empirical,<sup>5,6</sup> give important insights into the physics behind jet noise radiation. The equivalent source model (ESM) developed in this paper is somewhat similar to acoustical holography,<sup>7</sup> in that it starts with measured data and then uses a mathematical model to predict the sound field at other locations.<sup>8</sup> This ESM is an extension of a previous model developed by Morgan *et al.*<sup>9</sup> Modifications have been made such that the selection of the modeling parameters is optimized using Bayesian methods. Initial application of this optimized algorithm for obtaining equivalent source distributions for the F-22A Raptor is presented in this paper. Although a more complete description of the experiment is given by Wall *et al.*<sup>10</sup>, essential details of the layout are illustrated in Fig. 1.

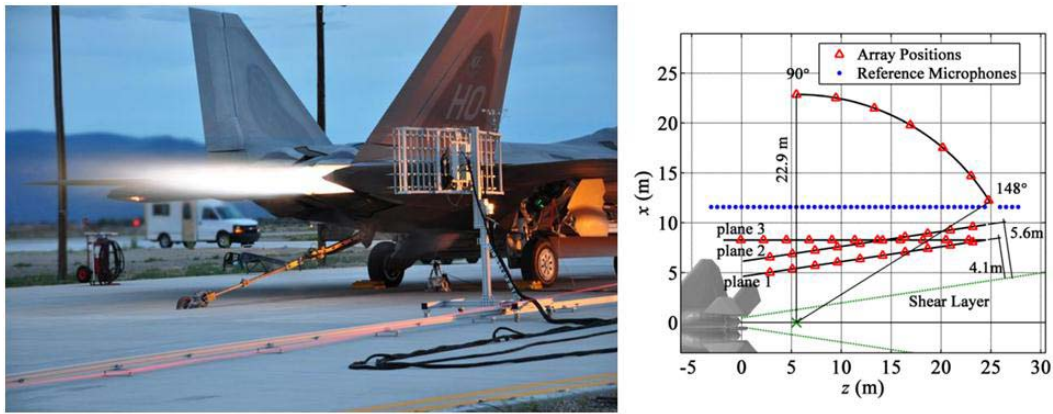


**FIGURE 1.** (left) A picture of the F22-A Raptor with the microphone array. (right) Schematic of the measurement locations relative to the jet. The red triangles indicate the locations at which the microphone array was positioned during the experiment. The estimated shear layer is marked by green dashed lines, and the green “x” delineates the estimated maximum-noise-source region and arc origin.

## EQUIVALENT SOURCE MODEL

In summary, this ESM is based on two line arrays of monopoles. One array is correlated while the other is uncorrelated, representing the two types of jet noise sources.<sup>11,12</sup> For each array, the relative amplitudes of the monopoles are given by a Rayleigh distribution, written as

$$|\tilde{A}_m(z_m, \Delta z, \sigma)| = A_{\max} \frac{z_m - \Delta z}{\sigma^2} e^{-\frac{(z_m - \Delta z)^2}{2\sigma^2}} = A_m(z_m, \Delta z, \sigma), \quad (1)$$

where  $z_m$  is the location of the  $m^{\text{th}}$  monopole,  $A_{\max}$  is the peak amplitude in the distribution,  $\Delta z$  is the distance the peak of the distribution has been shifted downstream, and  $\sigma$  is the relative width of the distribution. As shown in Fig. 2, the shift distance,  $\Delta z$ , corresponds with the placement of the peak in the Rayleigh distribution downstream to desired location,  $z_p$ . In addition, the monopoles in the correlated array have a phase difference from one monopole to the next which is

$$\varphi = \frac{-2\pi f d \cos \theta}{c}. \quad (2)$$

The space between the monopoles,  $d$ , is small enough to simulate a continuous source, and the sound speed is represented by the variable  $c$ . The source phase angle  $\theta$  can be obtained from analyzing a jet’s far-field directivity

pattern or can be included as an independent parameter.<sup>13</sup> The source phase angle is a function of the engine power and frequency.

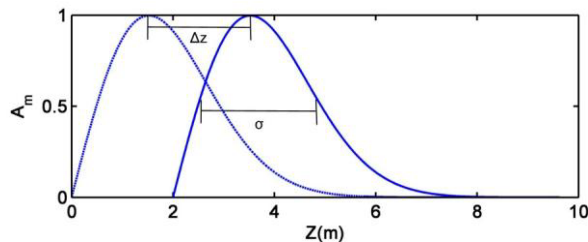


**FIGURE 2.** A Rayleigh distribution (dotted line), which rises quickly and decays slowly, and a shifted distribution (solid line), labeled with the shift distance,  $\Delta z$ , and the standard deviation,  $\sigma$ .

The parameters that control the maximum amplitude, the width, and the location of the peak for the correlated (subscript  $c$ ) and the uncorrelated (subscript  $u$ ) distributions are varied in the ESM. Specifically, the peak locations  $\{z_{p,u}, z_{p,c}\}$ , widths  $\{\sigma_u, \sigma_c\}$ , and the ratio of the maximum amplitudes of the two arrays  $\{A_{m,c}/A_{m,u}\}$  are variables. In addition, since the publication by Morgan *et al.*,<sup>9</sup> it was decided to include the source phase angle,  $\theta$ , as a variable as well.

### Automation of Parameter Selection

In order to find the best-fit parameters in the ESM efficiently, it is necessary to use an automated process. A Bayesian-based optimization algorithm (BOA) was used, which has shown to be effective in searching multidimensional parameter spaces, including applications in acoustics.<sup>14, 15, 16</sup> The BOA computes the fit between data and a model and provides both an optimal solution and the relative sensitivity of the match on the individual parameters. The first step is to use simulated annealing (SA) to find parameter estimates that optimize the match between the model and the data. The acceptance criteria within the SA search have some randomness to allow the algorithm to jump out of local minimums during the earlier parts of the algorithm. The SA algorithm typically runs about 10,000 times before converging to a solution. The final estimated parameter values are then used as the starting location for a fast Gibbs sampler (FGS).

The FGS algorithm is very similar to the SA algorithm, but the FGS algorithm is designed to sample the parameter space more equally, and thus yields insight into the uncertainty of the solution by providing estimates of the posterior probability distribution (PPD) for each parameter. The sets of parameters that were accepted during the FGS are stored and used to estimate the PPDs by plotting the value of a parameter versus the number of times it was selected, essentially as a histogram. An example of the estimated PPDs generated from the FGS is shown in Fig. 3. The width of a PPD indicates the sensitivity of the model-data mismatch to variations in that parameter across the multidimensional space. A well-defined peak in a PPD indicates that varying the parameter over the specified bounds impacts the ability of the model to predict the data, and thus, the value of that parameter estimated by the SA has an uncertainty specified by the width of the distribution. Conversely, a flat PPD shows that the match between the model and data, as defined in the error function, is not influenced by changes in that parameter across the specified bounds, and the corresponding estimated parameter value from the SA is not meaningful.

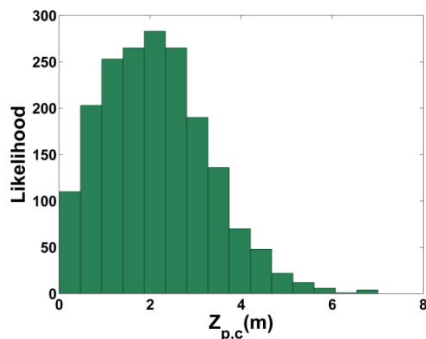


**FIGURE 3.** An estimated posterior probability distribution (PPD) from the fast Gibbs sampler. The peak of the PPD represents the most likely estimate of the modeling parameter  $z_{p,c}$ , and the width of the PPD is tied to the uncertainty in that estimate.

## RESULTS

After the BOA was fully functional and tested, estimates for the equivalent source model were generated using the F-22 data recorded at military power and afterburner for the following one-third octave band center frequencies: 100 Hz, 125 Hz, 200 Hz, 315 Hz, 800 Hz, and 1250 Hz. The estimated equivalent source parameters were evaluated in three ways. First, the PPDs from the FGS were analyzed to determine which parameter estimates were physically meaningful. Second, the resulting source distributions were compared to the current understanding of jet noise source characteristics. Third, the estimated equivalent source distributions were used in the radiation model to calculate the sound field at two of the measurement locations: the plane 4.1 m from the shear layer, which was used to create the ESM, and the arc 23 m from the estimated maximum source region. (See Fig. 1.) The comparison between  $\bar{P}_{r,i}$ , the reference pressure from the measured data, and  $\bar{P}_{m,i}$ , the modeled pressure at measurement location  $i$ , across the  $\tilde{N}$  measurement locations within 25 dB of the maximum level was calculated as

$$\text{Error} = \frac{1}{\tilde{N}} \frac{\sum_{i=1}^{\tilde{N}} |\bar{P}_{r,i}^2 - \bar{P}_{m,i}^2|^2}{\max(\bar{P}_r^2)}. \quad (3)$$

An analysis of the PPDs corresponding to the parameters of the ESM provides insights into the uncertainties associated with the estimated source distributions obtained by the optimization. The PPDs for 315 Hz at afterburner, shown in Fig. 4, are representative of those produced for the other frequencies and engine conditions. From the shape of the PPDs, it is evident that the parameters associated with the correlated source (the peak and width of the amplitude distribution) have a significant influence on the match between the data and the model. This indicates that the parameter estimates are meaningful to within the uncertainty indicated by the PPDs. This is as expected due to the fact that the correlated sources account for the higher levels in the sound field. On the other hand, the flatness of the PPDs for the parameters of the uncorrelated source distribution means that the agreement between the model and the top 25 dB of the data is largely insensitive to changes in these parameters. Thus, the uncertainties associated with the estimates for  $z_{p,u}$  and  $\sigma_u$  are so large that they are not physically meaningful. Also, the phase angle,  $\theta$ , has a large effect on the predicted sound field.

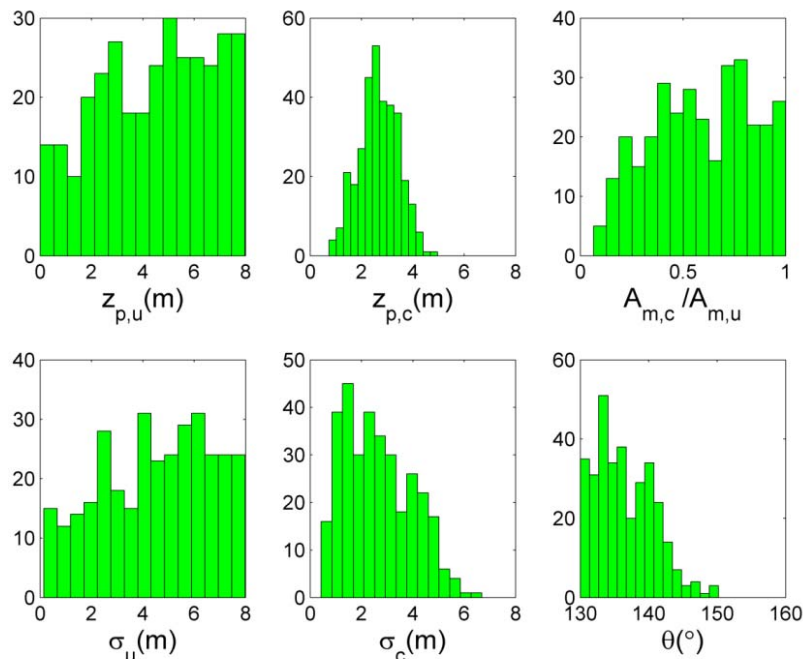


**FIGURE 4.** The PPDs for the 315-Hz one-third octave band at afterburner for the ESM:  $z_{p,u}$  and  $\sigma_u$  are the peak and width of the uncorrelated source distribution, respectively.  $z_{p,c}$  and  $\sigma_c$  are the peak and width of the correlated source distribution respectively.  $A_{m,c}/A_{m,u}$  is the ratio of the amplitudes of the two distributions.  $\theta$  is the source phase angle.

Next, some conclusions can also be made from analyzing the ESM distributions that were generated by the optimization. As described above, the uncertainties in the uncorrelated source distributions are very large because the uncorrelated sources have little effect on the overall sound field. For this reason, they are not included in the results shown here. In the correlated source distributions shown in Fig. 5 and Table 1,  $z_{p,c}$  approaches the jet nozzle as the frequency increases. In addition,  $\sigma_c$  appears to narrow as frequency increases. Also, the angle seems to stay fairly close to  $135^\circ \pm 5^\circ$  degrees, as expected from the PPD.

Finally, conclusions can be made by comparing the predicted near- and far-field levels with the measured data. Figures 6-9 contain predicted and measured levels on the 4.1-m plane, used to obtain the source parameters, and along the 23 m arc for the 125, 200, 315, and 1250 Hz bands. In general, agreement in the maximum source region at both locations is within 1-2 dB. However, the agreement in the low-amplitude portions near the ground reflection nulls and along the edges worsens, particularly for the 1250 Hz case displayed in Fig. 9. The model assumes a perfectly coherent interaction from the line source with its image, and consequently predicts very deep nulls. However, the jet is an extended volumetric source, with likely partially incoherent reflections occurring, which lessen the depths of the nulls. The over prediction, particularly downstream of the maximum radiation region, seems to be caused by the long tails associated with the Rayleigh distribution. As the frequency increases, it is likely that the shape of the distribution fundamentally changes, which is not accounted for in the current ESM.

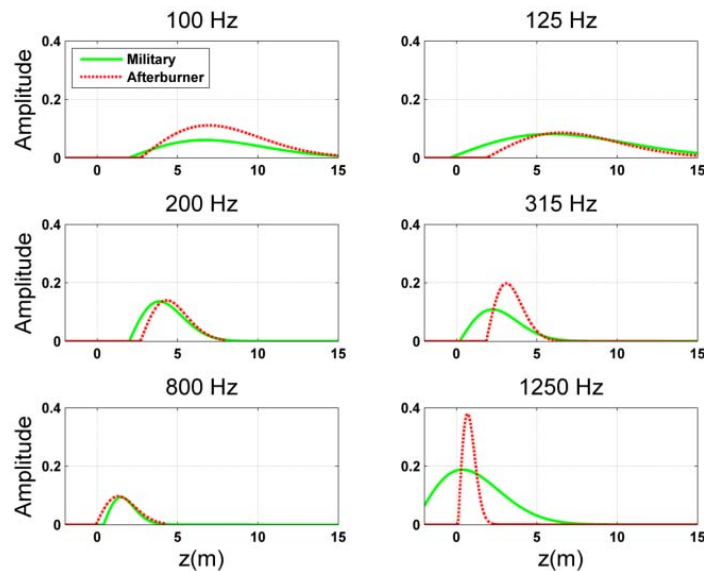
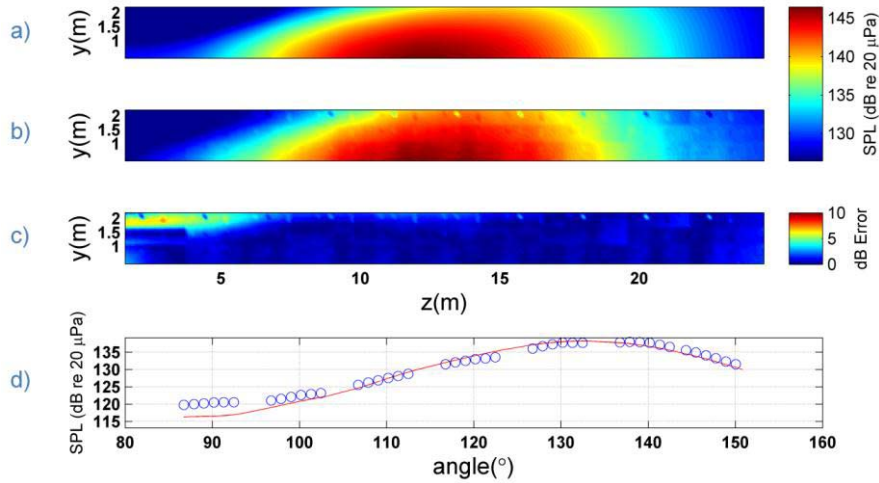


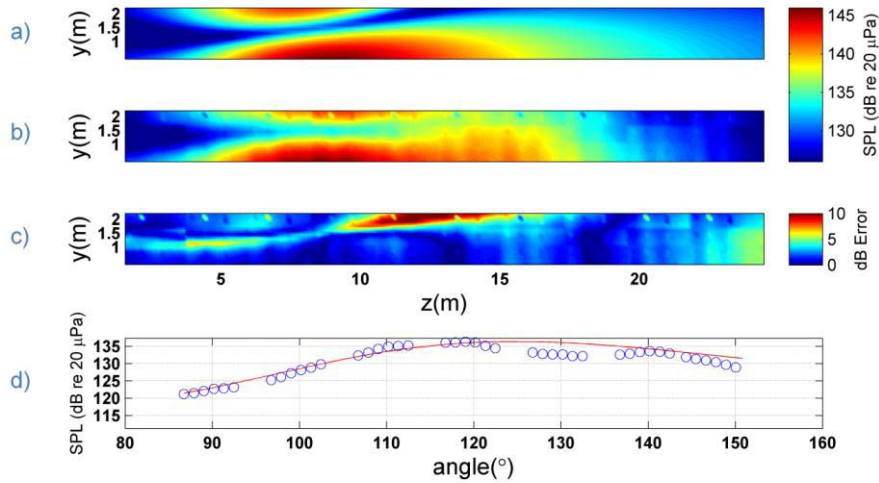
FIGURE 5. Equivalent source distributions at military and afterburner for different frequencies.

TABLE 1. Phase angle and peak locations of the equivalent correlated sources for afterburner and military engine powers at various frequencies.

Frequency	Military $\theta$ (degrees)	Military $z_{p,c}$ (m)	Afterburner $\theta$ (degrees)	Afterburner $z_{p,c}$ (m)
100 Hz	137.5	6.7	130.0	6.9
125 Hz	141.5	5.9	132.0	6.5
200 Hz	134.5	3.9	130.5	4.3
315 Hz	140.0	2.3	132.5	3.1
800 Hz	131.0	1.5	130.5	1.3
1250 Hz	137.5	0.4	131.0	0.7



**FIGURE 6.** Comparison of the ESM field and measured data for 125 Hz at afterburner. The following data are shown: a) the modeled SPL at 4.1-m from the shear layer, b) the measured SPL at the same location, c) the decibel difference between (a) and (b) (Near-field error = 0.0009), and d) the modeled SPL (red line) and the measured SPL (blue circles) along the 23-m arc (far-field error = 0.0071).



**FIGURE 7.** Comparison of the ESM field and measured data for 200 Hz at afterburner. For plot descriptions, see Fig. 6. Error in the near field is 0.0045. Error in the far field is 0.0539.

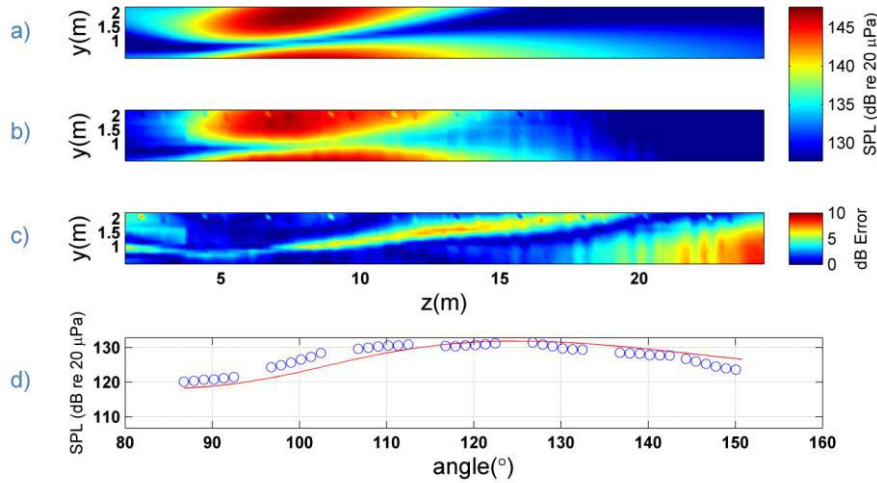


**FIGURE 8.** Comparison of the ESM field and measured data for 315 Hz at afterburner. For plot descriptions, see Fig. 6. Error in the near field is 0.0041. Error in the far field is 0.360.

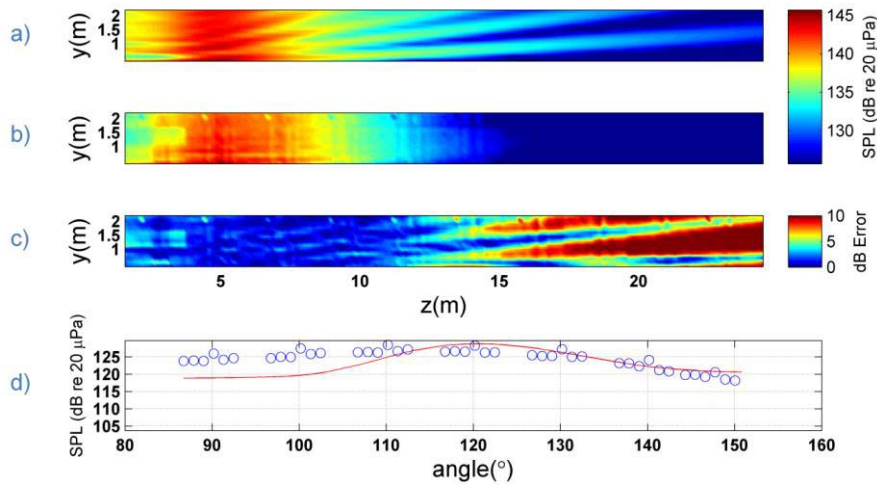


**FIGURE 9.** Comparison of the ESM fields and measured data for 1250 Hz at afterburner. For plot descriptions, see Fig. 6. Error in the near field is 0.0058. Error in the far field is 0.0743.

## CONCLUSION

The previous implementation of an equivalent source model for the F-22A Raptor by Morgan *et al.*<sup>9</sup> used manual adjustment of parameters and a fixed source phase angle derived from far-field directivity measurements. In this paper, we have shown a successful implementation of a robust Bayesian-based parameter optimization method that not only predicts the measured radiation along a near-field measurement plane, but also shows that the optimized parameters can be used in a simple-source model to estimate the far-field levels with reasonable accuracy.

## ACKNOWLEDGEMENTS

The authors gratefully acknowledge funding for this analysis from the Office of Naval Research. The measurements were funded by the Air Force Research Laboratory through the SBIR program and supported through a Cooperative Research and Development Agreement (CRADA) between Blue Ridge Research and Consulting, Brigham Young University, and the Air Force.<sup>17,18</sup> The authors also recognize the contributions of Dan Santos with the 508 ASW/YF at Hill Air Force Base and Senior Master Sergeant Neil Raben and the 49th Fighter Wing at Holloman Air Force Base in completing the experiment.

## REFERENCES

- 
- <sup>1</sup> J. Bridges and M. Wernet, "Measurements of the aeroacoustic sound source in hot jets," NASA/TM – 2004-212508, NASA Glenn Research Center, Cleveland, OH, Feb. 2004.
  - <sup>2</sup> V. Fleury, C. Bailly, E. Jondeau, M. Michard, and D. Juvé, "Space-time correlations in two subsonic jets using dual particle velocimetry measurements," *AIAA J.* **46**, 2498-2509 (2008).
  - <sup>3</sup> C. Bailly, P. Lafon, and S. Candel, "Subsonic and supersonic jet noise predictions from statistical source models," *AIAA J.* **35**, 1688-1696 (1997).
  - <sup>4</sup> C. K. W. Tam, N. N. Pastouchenko, and K. Viswanathan, "Extension of the near acoustic field of a jet to the far field," *Procedia IUTAM* **1**, 9-18 (2010).
  - <sup>5</sup> K. Viswanathan, "Mechanisms of jet noise generation: Classical theories and recent developments," *Int. J. of Aeroacoustics* **8**, 355-407 (2009).
  - <sup>6</sup> A. Bassetti, M. J. Fisher, and C. L. Morfey, "A semi-empirical model of jet noise prediction in the geometric near field, AIAA paper 2004-2831, May 2004.
  - <sup>7</sup> M. Lee and J. S. Bolton, "Source characterization of a subsonic jet by using near-field acoustical holography," *J. Acoust. Soc. Am.* **121**, 967-977 (2007).
  - <sup>8</sup> M. Ochmann, "The source simulation technique for acoustic radiation problems," *Acustica* **81**, 512-527 (1995).
  - <sup>9</sup> J. Morgan, T. B. Neilsen, K. L. Gee, A. T. Wall, and M. M. James, "Simple-source model of high-power jet aircraft noise," *Noise Control Eng. J.* **60**, 435-449 (2012).
  - <sup>10</sup> A. T. Wall, K. L. Gee, M. M. James, K. A. Bradley, S. A. McInerny, and T. B. Neilsen, "Near-field noise measurements of a high-power jet aircraft," *Noise Control Eng. J.* **60**, 421-434 (2012).
  - <sup>11</sup> C. K. W. Tam, K. Viswanathan, K. K. Ahuja, and J. Panda, "The sources of jet noise: experimental evidence," *J. Fluid Mech.*, **615**, 253-292 (2008).
  - <sup>12</sup> C. K. W. Tam, M. Golebiowski, J. M. Seiner, "On the Two Components of Turbulent Mixing Noise from Supersonic Jets," AIAA paper 96-1716.
  - <sup>13</sup> A sine function appears in the original publication of Ref [9]. However, a cosine corrects for an ambiguity in the reference point.
  - <sup>14</sup> M. K. Sen and P. L. Stoffa, "Bayesian inference, Gibbs sampler and uncertainty estimation in geophysical inversion," *Geophys. Prospect.* **44**, 313-350 (1996).
  - <sup>15</sup> K. Yang, N. R. Chapman, Y. Ma, "Estimating parameter uncertainties in matched field inversion by a neighborhood approximation algorithm," *J. Acoust. Soc. Am.* **121**, 833-843 (2007).
  - <sup>16</sup> J. Chazot, E. Zhang, J. Antoni, "Acoustical and mechanical characterization of poroelastic materials using a Bayesian approach," *J. Acoust. Soc. Am.* **131**, 4584-4595 (2012).
  - <sup>17</sup> SBIR DATA RIGHTS - (DFARS 252.227-7018 (JUNE 1995)); Contract Number: FA8650-08-C-6843; Contractor Name and Address: Blue Ridge Research and Consulting, LLC, 15 W Walnut St. Suite C; Asheville, NC Expiration of SBIR Data Rights Period: March 17, 2016 (Subject to SBA SBIR Directive of September 24, 2002) *The Government's rights to use, modify, reproduce, release, perform, display, or disclose technical data or computer software marked with this legend are restricted during the period shown as provided in paragraph (b)(4) of the Rights in Noncommercial Technical Data and Computer Software—Small Business Innovation Research (SBIR) Program clause contained in the above identified contract. No restrictions apply after the expiration date shown above. Any reproduction of technical data, computer software, or portions thereof marked with this legend must also reproduce the markings.*
  - <sup>18</sup> Distribution A – Approved for public release; Distribution is unlimited 88ABW-2012-6365.